Environment-Induced Sudden Death of Entanglement

M. P. Almeida, *et al.*

Science **316**, 579 (2007);
DOI: 10.1126/science.1139892

Science (print ISSN 0036-8075; online ISSN 1095-9203) is published weekly, except the last week in December, by the American Association for the Advancement of Science, 1200 New York Avenue NW, Washington, DC 20005.

absence of miR-208, the expression of β*MHC* is severely blunted in the adult heart in response to pressure overload, activated calcineurin, or hypothyroidism, suggesting that the pathways through which these stimuli induce β*MHC* transcription share a common miR-208–sensitive component (Fig. 6). In contrast, β*MHC* expression was unaltered in the hearts of newborn miR-208$^{-/-}$ mice, demonstrating that miR-208 participates specifically in the mechanism for stress-dependent regulation of β*MHC* expression.

A clue to the mechanism of action of miR-208 comes from the resemblance of miR-208$^{-/-}$ hearts to hyperthyroid hearts, both of which display a block to βMHC expression, up-regulation of stress-response genes (*29*, *30*), and protection against pathological hypertrophy and fibrosis (*31*, *32*). The up-regulation of fast skeletal muscle genes in miR-208$^{-/-}$ hearts also mimics the induction of fast skeletal muscle fibers in the hyperthyroid state (*33*). T3 signaling represses β*MHC* expression in the postnatal heart, and PTU, which causes hypothyroidism, induces β*MHC* (*2*, *21*). The inability of PTU to induce β*MHC* expression in miR-208$^{-/-}$ hearts further implicates miR-208 in the T3 signaling pathway.

Our results suggest that miR-208 acts, at least in part, by repressing expression of the TR coregulator THRAP1, which can exert positive and negative effects on transcription (*34*, *35*). The TR acts through a negative TRE to repress β*MHC* expression in the adult heart (*2*). Thus, the increase in THRAP1 expression in the absence of miR-208 would be predicted to enhance the repressive activity of the TR toward β*MHC* expression, consistent with the blockade to β*MHC* expression in miR-208$^{-/-}$ hearts. In contrast, the regulation of α*MHC* and β*MHC* expression during development is independent of T3 signaling (*2*) and is unaffected by miR-208. Notably, other TR target genes, such as *phospholamban* and *sarco(endo)plasmic reticulum calcium ATPase 2a* and *glucose transporter 4* were expressed normally in miR-208$^{-/-}$ mice (fig. S7). It has been proposed that the β*MHC* gene may respond to specific TR isoforms (*36*–*38*). Perhaps THRAP1 acts on specific TR isoforms or selectively on a subset of TR-dependent genes through interactions with promoter-specific factors. Because miRNAs generally act through multiple downstream targets to exert their effects, additional targets are also likely to contribute to the effects of miR-208 on cardiac growth and gene expression.

Relatively minor increases in βMHC composition, as occur during cardiac hypertrophy and heart failure, can reduce myofibrillar ATPase activity and systolic function (*9*). Thus, therapeutic manipulation of miR-208 expression or interaction with its mRNA targets could potentially enhance cardiac function by suppressing βMHC expression. Based on the profound influence of miR-208 on the cardiac stress response, and the regulation of numerous miRNAs in the diseased heart (*19*), we anticipate that miRNAs will prove to be key regulators of the functions and responses to disease of the adult heart and possibly other organs.

References and Notes

1. A. Weiss, L. A. Leinwand, *Annu. Rev. Cell Dev. Biol.* **12**, 417 (1996).
2. E. Morkin, *Microsc. Res. Tech.* **50**, 522 (2000).
3. M. Krenz, J. Robbins, *J. Am. Coll. Cardiol.* **44**, 2390 (2004).
4. H. Kiriazis, E. G. Kranias, *Annu. Rev. Physiol.* **62**, 321 (2000).
5. D. Fatkin *et al.*, *J. Clin. Invest.* **106**, 1351 (2000).
6. B. D. Lowes *et al.*, *J. Clin. Invest.* **100**, 2315 (1997).
7. S. Miyata, W. Minobe, M. R. Bristow, L. A. Leinwand, *Circ. Res.* **86**, 386 (2000).
8. K. Nakao, W. Minobe, R. Roden, M. R. Bristow, L. A. Leinwand, *J. Clin. Invest.* **100**, 2362 (1997).
9. W. T. Abraham *et al.*, *Mol. Med.* **8**, 750 (2002).
10. T. A. McKinsey, E. N. Olson, *J. Clin. Invest.* **115**, 538 (2005).
11. D. P. Bartel, *Cell* **116**, 281 (2004).
12. W. P. Kloosterman, R. H. Plasterk, *Dev. Cell* **11**, 441 (2006).
13. A. Esquela-Kerscher, F. J. Slack, *Nat. Rev. Cancer* **6**, 259 (2006).
14. S. Costinean *et al.*, *Proc. Natl. Acad. Sci. U.S.A.* **103**, 7024 (2006).
15. S. M. Hammond, *Curr. Opin. Genet. Dev.* **16**, 4 (2006).
16. V. Ambros, *Cell* **113**, 673 (2003).
17. Y. Zhao, E. Samal, D. Srivastava, *Nature* **436**, 214 (2005).
18. J. F. Chen *et al.*, *Nat. Genet.* **38**, 228 (2006).
19. E. van Rooij *et al.*, *Proc. Natl. Acad. Sci. U.S.A.* **103**, 18255 (2006).
20. A. Subramaniam *et al.*, *J. Biol. Chem.* **266**, 24613 (1991).
21. G. T. Schuyler, L. R. Yarbrough, *Basic Res. Cardiol.* **85**, 481 (1990).
22. W. K. Jones *et al.*, *J. Clin. Invest.* **98**, 1906 (1996).
23. J. A. Hill *et al.*, *Circulation* **101**, 2863 (2000).
24. J. D. Molkentin *et al.*, *Cell* **93**, 215 (1998).
25. K. Ojamaa, A. Kenessey, I. Klein, *Endocrinology* **141**, 2139 (2000).
26. A. Krek *et al.*, *Nat. Genet.* **37**, 495 (2005).
27. M. Ito, R. G. Roeder, *Trends Endocrinol. Metab.* **12**, 127 (2001).
28. A. K. Leung, J. M. Calabrese, P. A. Sharp, *Proc. Natl. Acad. Sci. U.S.A.* **103**, 18125 (2006).
29. T. Wei, C. Zeng, Y. Tian, Q. Chen, L. Wang, *J. Endocrinol. Invest.* **28**, 8 (2005).
30. C. Pantos *et al.*, *Horm. Metab. Res.* **38**, 308 (2006).
31. J. Yao, M. Eghbali, *Circ. Res.* **71**, 831 (1992).
32. W. J. Chen, K. H. Lin, Y. S. Lee, *Mol. Cell. Endocrinol.* **162**, 45 (2000).
33. A. Vadaszova, G. Zacharova, K. Machacova, I. Jirmanova, T. Soukup, *Physiol. Res.* **53**, (suppl. 1), S57 (2004).
34. R. Pavri *et al.*, *Mol. Cell* **18**, 83 (2005).
35. S. W. Park *et al.*, *Mol. Cell* **19**, 643 (2005).
36. K. Kinugawa, C. S. Long, M. R. Bristow, *J. Clin. Endocrinol. Metab.* **86**, 5089 (2001).
37. A. Mansen, F. Yu, D. Forrest, L. Larsson, B. Vennstrom, *Mol. Endocrinol.* **15**, 2106 (2001).
38. K. Kinugawa *et al.*, *Circ. Res.* **89**, 591 (2001).

39. This work was supported by grants from the NIH and the Donald W. Reynolds Cardiovascular Clinical Research Center to E.N.O. We thank C. Plato at Gilead Colorado (Westminster, CO) for providing human and rat RNA samples; M. Arnold for advice; and J. Shelton, J. McAnally, and C. Nolen for technical assistance.

Supporting Online Material

www.sciencemag.org/cgi/content/full/1139089/DC1
Materials and Methods
Figs. S1 to S7
Tables S1 and S2
References

20 December 2006; accepted 7 March 2007
Published online 22 March 2007;
10.1126/science.1139089
Include this information when citing this paper.

REPORTS

Environment-Induced Sudden Death of Entanglement

M. P. Almeida, F. de Melo, M. Hor-Meyll, A. Salles, S. P. Walborn, P. H. Souto Ribeiro, L. Davidovich*

We demonstrate the difference between local, single-particle dynamics and global dynamics of entangled quantum systems coupled to independent environments. Using an all-optical experimental setup, we showed that, even when the environment-induced decay of each system is asymptotic, quantum entanglement may suddenly disappear. This "sudden death" constitutes yet another distinct and counterintuitive trait of entanglement.

The real-world success of quantum computation (*1*, *2*) and communication (*3*–*9*) relies on the longevity of entanglement in multiparticle quantum states. The presence of decoherence (*10*) in communication channels and computing devices, which stems from the unavoidable interaction between these systems and the environment, degrades the entanglement when the particles propagate or the computation evolves. Decoherence leads to local dynamics, associated with single-particle dissipation, diffusion, and decay, as well as to global dynamics, which may provoke the disappearance of entanglement at a finite time (*11*–*15*). This phenomenon, known as "entanglement sudden death" (*15*), is strikingly different from single-particle dynamics, which occurs asymptotically, and has thus stimulated much recent theoretical work (*11*–*15*). Here we demonstrate the sudden death of entanglement of a two-qubit system under the influence of independent environ-

Instituto de Física, Universidade Federal do Rio de Janeiro, Caixa Postal 68528, Rio de Janeiro RJ 21941-972, Brazil.

*To whom correspondence should be addressed. E-mail: ldavid@if.ufrj.br

ments. Our all-optical setup allows for the controlled investigation of a variety of dynamical maps that describe fundamental processes in quantum mechanics and quantum information.

Consider a two-level quantum system S (upper and lower states $|e\rangle$ and $|g\rangle$, respectively) under the action of a zero-temperature reservoir R. At zero temperature, the reservoir R is in the $|0\rangle_R$ (vacuum) state, and the S-R interaction can be represented by a quantum map, known as the amplitude decay channel (*1*):

$$\begin{aligned} |g\rangle_S\otimes|0\rangle_R &\rightarrow |g\rangle_S\otimes|0\rangle_R \\ |e\rangle_S\otimes|0\rangle_R &\rightarrow \sqrt{1-p}|e\rangle_S\otimes|0\rangle_R + \sqrt{p}|g\rangle_S\otimes|1\rangle_R \end{aligned} \quad (1)$$

Under this map, the lower state $|g\rangle$ is not affected while the upper state $|e\rangle$ either decays to $|g\rangle$ with probability p, creating one excitation in the environment (state $|1\rangle_R$), or remains in $|e\rangle$, with probability $1 - p$. This would be the situation, for instance, in the spontaneous emission of a two-level atom. In this case, the state $|1\rangle_R$ would correspond to one photon in the reservoir. Under the Markovian approximation, $p = 1 - \exp(-\Gamma t)$, that is, the decay probability approaches unity exponentially in time. As an initial pure state $a|e\rangle + b|g\rangle$ decays, it gets entangled with the environment, gradually losing its coherence and its purity over time. Complete decay only occurs asymptotically in time ($p \rightarrow 1$ when $t \rightarrow \infty$), when the two-level system is again described by the pure state $|g\rangle$. Note that the map in Eq. 1 encompasses several other kinds of dynamics, which differ only by the time dependence of the parameter p.

Now consider two entangled qubits that decay according to this map. How does the entanglement of the two-qubit system evolve? Does it mimic the asymptotic decay of each qubit, disappearing at $t \rightarrow \infty$, or does it disappear at some finite time? This question has been explored theoretically (*11*–*15*), but up to now there has been no experimental investigation of the relation between the global entanglement dynamics and the local decay of the constituent subsystems.

To answer these questions, one first needs a formal definition of entanglement. A two-qubit pure state is entangled, or nonseparable, if and only if the total state cannot be expressed as a product of the individual qubit states: $|\psi\rangle \neq |\phi\rangle_1\otimes|\varphi\rangle_2$. Likewise, a mixed bipartite state represented by a density matrix ρ is separable if and only if it can be written as a convex sum of products of individual density matrices: $\rho = \sum_i p_i \rho_i^{(1)}\otimes\rho_i^{(2)}$, with $0 \leq p_i \leq 1$. A convenient measure of entanglement for a two-qubit state ρ is the concurrence C (*16*), given by

$$C = \max\{0, \Lambda\} \quad (2)$$

where

$$\Lambda = \sqrt{\lambda_1} - \sqrt{\lambda_2} - \sqrt{\lambda_3} - \sqrt{\lambda_4} \quad (3)$$

and the quantities λ_i are the positive eigenvalues, in decreasing order, of the matrix

$$\rho(\sigma_y\otimes\sigma_y)\rho^*(\sigma_y\otimes\sigma_y) \quad (4)$$

where σ_y is the second Pauli matrix and the conjugation occurs in the computational basis $\{|00\rangle, |01\rangle, |10\rangle, |11\rangle\}$. C quantifies the amount of quantum correlation that is present in the system and can assume values between 0 (only classical correlations) and 1 (maximal entanglement).

For the dynamics given by Eq. 1 and an initial state of the form $|\Phi\rangle = |\alpha||gg\rangle + |\beta|\exp(i\delta)|ee\rangle$, the entanglement decay dynamics depends on the relation between $|\alpha|$ and $|\beta|$ (*14*). Concurrence in this case is given by

$$C = \max\{0, 2(1-p)|\beta|(|\alpha| - p|\beta|)\} \quad (5)$$

From this expression, one can see that for $|\beta| \leq |\alpha|$, entanglement disappears only when the individual qubits have completely decayed ($p = 1$), whereas for $|\beta| > |\alpha|$, entanglement disappears for $p = |\alpha/\beta| < 1$, which corresponds to a finite time. This phenomenon has been called "entanglement sudden death" (*15*). Because the concurrence of the initial state ($p = 0$) is $C = 2|\alpha\beta|$, the entanglement dynamics of two states with the same initial concurrence can be quite different.

Photons are a useful experimental tool for demonstrating these properties and, more generally, for studying quantum channels like the one given in Eq. 1, as the decoherence mechanisms can be implemented in a controlled manner. Let us associate the H and V polarizations of a photon, respectively, to the ground and excited states of the two-level system S. The reservoir R in turn is represented by two different momentum modes of the photon.

Figure 1A shows a Sagnac-like interferometer that implements the amplitude-decay channel 1 for a single qubit. A photon, initially in the incoming part of mode a, is split into its horizontal (H) and vertical (V) polarization components by a polarizing beam splitter (PBS1). Let us ignore the half-wave plates HWP1 and HWPC momentarily. The V-polarization component is reflected and propagates through the interferometer in the clockwise direction, and, if unaltered, reflects through PBS1 into the outgoing part of mode a. The H-polarization component is transmitted and propagates through the interferometer in the counterclockwise direction and transmits through PBS1, also into the outgoing part of mode a (*17*). The interferometer is aligned so that the two paths are spatially separated, making it possible to manipulate the H and V polarization components independently.

To realize the amplitude decay given in Eq. 1, we use HWP1 to rotate the polarization of the V component to $\cos(2\theta)|V\rangle + \sin(2\theta)|H\rangle$, where θ is the angle of HWP1. Suppose that an incoming photon is V-polarized. When this photon exits the interferometer through PBS1, it is transmitted into mode b with probability $p = \sin^2(2\theta)$ and reflected into mode a with prob-

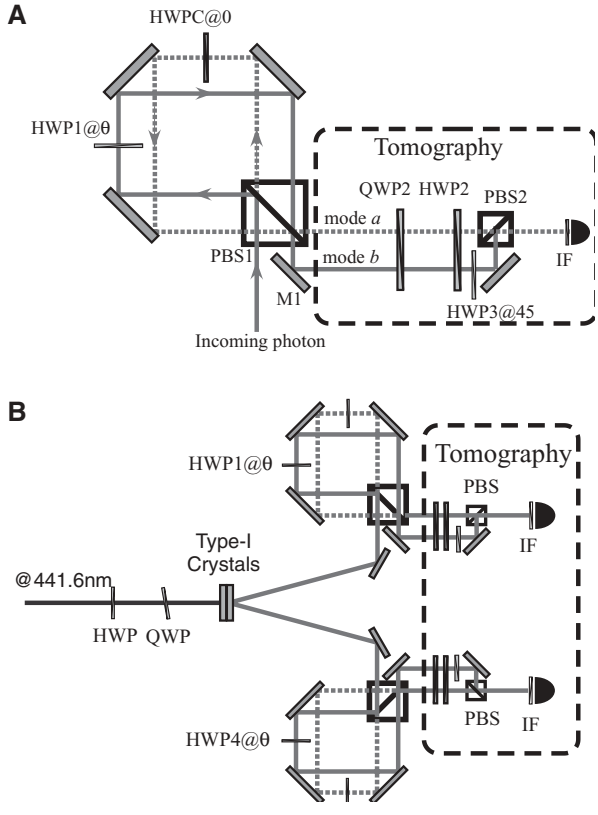

Fig. 1. Experimental setup. (**A**) Amplitude decay channel for a single photonic qubit. Because of the polarized beam splitter PBS1, the H and V components of polarized photons respectively propagate along counterclockwise and clockwise paths within the interferometer. With half-wave plate HWP1 set at 0°, they are coherently recombined into the outgoing spatial mode a, which represents the "vacuum state" of the reservoir. For other angles of HWP1, the V component undergoes a rotation, corresponding to its probabilistic "decay" into the H component, which PBS1 sends to outgoing mode b, representing the "one-excitation state" of the reservoir. Wave plates HWP2 and QWP2, together with PBS2, are used for tomography of the polarization state of outgoing modes a and b, which are recombined incoherently on PBS2 through HWP3 and are sent to the same detector. IF is an interference filter. (**B**) Amplitude decay channel applied to entangled qubits. The entangled state is generated by parametric down-conversion in type I nonlinear crystals.

ability $\cos^2(2\theta)$. This evolution can thus be described by $|V\rangle|a\rangle \rightarrow \sqrt{(1-p)}|V\rangle|a\rangle + \sqrt{p}|H\rangle|b\rangle$. Identifying the outgoing modes a and b (which correspond to orthogonal spatial modes) as the states of the reservoir with zero and one excitation, respectively, this operation is equivalent to that on the $|e\rangle|0\rangle_R$ state in Eq. 1. An incoming H-polarized photon is left untouched, corresponding to the first line in Eq. 1. This process therefore realizes the amplitude decay channel and is identical to the decay of a two-level system. Half-wave plate HWPC, oriented at 0°, is used solely to match the lengths of the two optical paths. The path lengths are adjusted so that if HWP1 is oriented at 0°, the polarization state in mode a after the interferometer is exactly the same as the input state. Photons in modes a and b are then directed to the same quantum state tomography (QST) system (*18*), composed of quarter-wave plate QWP2, half-wave plate HWP2, and polarizing beam splitter PBS2, and then registered using a single-photon detector equipped with a 10-nm (full width at half maximum) interference filter and a 1.5-mm-diameter aperture. Mode b is recombined incoherently with mode a on PBS2, so that both modes can be detected with a single detector. This is achieved by assuring that the path length difference between modes a and b is greater than the coherence length of the photons, which is determined by the width of the interference filters (~0.1 mm). The half-wave plate HWP3, aligned at 45°, transforms H-polarized photons into V-polarized ones. Because PBS2 transmits H-polarization and reflects V-polarization, the combination of HWP3 and PBS2 reflects photons that were originally H-polarized. This assures that the QST performed is identical for both modes a and b.

Using the interferometer described above, we studied both the decay of a single qubit and the dynamics of two entangled two-level systems interacting with independent amplitude-decay reservoirs. In the experimental setup (Fig. 1B), polarization-entangled photon pairs with wavelength centered around 884 nm were produced using a standard source (*19*) composed of two adjacent type-I $LiIO_3$ nonlinear crystals pumped by a 441.6-nm continuous-wave He-Cd laser. One crystal produces photon pairs with V-polarization and the other produces pairs with H-polarization. After propagation and spatial mode filtering, the H and V modes are spatially indistinguishable, and a photon pair is described by the pure state $|\Phi\rangle = |\alpha||HH\rangle + |\beta| \exp(i\delta) |VV\rangle$ with high fidelity. A half-wave plate and a quarter-wave plate placed in the pump beam (Fig. 1B, left) allow the control of the coefficients $|\alpha|$ and $|\beta|$ and the relative phase δ of the state (*19*).

The decay of a single qubit was investigated experimentally for both H- and V-polarized photons by generating states $|VV\rangle$ and $|HH\rangle$ and registering coincidence counts, with one photon propagating through the interferometer and the other serving as a trigger. The coincidence detection window ($c \times 5$ ns ~ 1.5 m) was larger than the path difference between outgoing modes a and b (~5 cm). Figure 2A shows $P_V(V)$, $P_H(V)$, $P_V(H)$, and $P_H(H)$ as a function of p, where $P_J(K)$ is the probability of finding an input K-polarized photon in the J state after the interferometer. The linear behavior in p is characteristic of exponential decay in t, if $p = 1 - \exp(-\Gamma t)$.

For the investigation of entanglement dynamics, nonmaximally entangled states were produced and each photon was sent to a separate interferometer, which implemented an amplitude-damping reservoir, and then to a QST system. The half-wave plates HWP1 and HWP4 were set to the same angle θ, so that the reservoirs, although independent, acted with the same probability p. QST of the two-photon state followed the usual recipe of 16 coincidence measurements (*18*). Each measurement lasted 90 s, giving an average of about 250 coincidence events. We repeated the same procedure for different values of p, obtaining the tomographic reconstruction of the output two-photon polarization state in all cases. The concurrence was calculated using Eqs. 2 and 3. In all figures, horizontal error bars represent uncertainty in aligning the wave plates, and vertical error bars correspond to the standard deviations of Monte Carlo samples obtained from randomly generated counts following the statistics of the experimental data (*20*).

Figure 2B displays the concurrence and the quantity Λ, given by Eq. 3, as a function of the decay probability p, for two initial states that, although not pure, are very close to $|\Phi\rangle = |\alpha||HH\rangle + |\beta| \exp(i\delta) |VV\rangle$: state I, defined by $|\beta|^2 = |\alpha|^2/3$ (triangles), and state II, defined $|\beta|^2 = 3|\alpha|^2$ (squares). Tomography of the initial states I and II showed them to have the same concurrence (~0.8) and similar purity (~0.91 to 0.97). The theoretical curves were obtained by applying Eq. 1 to the experimentally determined initial states, which correspond to $p = 0$. For initial state I, entanglement disappears asymptotically, and the concurrence goes to zero only when both individual systems have decayed completely ($p = 1$).

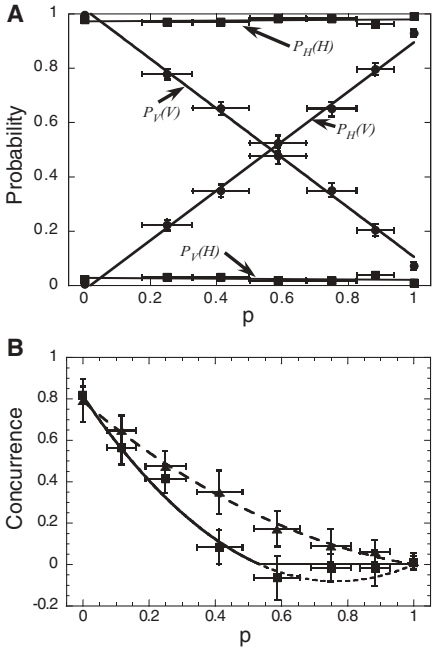

Fig. 2. Results for amplitude decay channel. (**A**) Experimental amplitude decay for a single qubit. $P_V(V)$ and $P_H(V)$ are the probabilities of detecting an input V-polarized photon in the V and H states, respectively; $P_V(H)$ and $P_H(H)$ are the probabilities for an input H-polarized photon. The points correspond to experimental data, and the lines are linear fits. (**B**) Entanglement decay as a function of the probability p. The squares correspond to experimentally obtained values of Λ for the case $|\beta|^2 = 3|\alpha|^2$. The solid line is the theoretical prediction of the concurrence for this state, given by Eq. 2; the dotted line shows the value of Λ, given by Eq. 3. The triangles are experimental values of Λ for the case $|\beta|^2 = |\alpha|^2/3$, and the dashed line is the theoretical prediction for Λ and C, which are equivalent for this state.

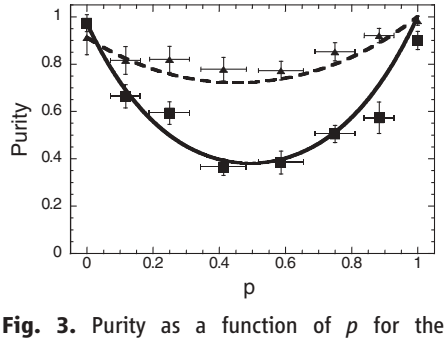

Fig. 3. Purity as a function of p for the amplitude damping channel. The squares correspond to experimentally obtained values of the purity for the case $|\beta|^2 = 3|\alpha|^2$; the solid line is the theoretical prediction. The triangles are experimental values of the purity for the case $|\beta|^2 = |\alpha|^2/3$, and the dashed line is the corresponding theoretical prediction.

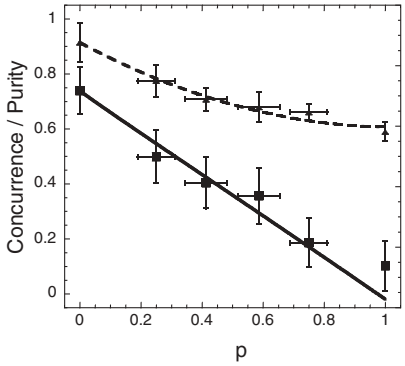

Fig. 4. Experimental results for the dephasing reservoir. Concurrence (squares) and purity (triangles) are shown for the case $|\beta|^2 = 3|\alpha|^2$. The solid line is the corresponding theoretical prediction for concurrence, given by Eq. 2. The dashed line is the theoretical prediction for purity, given by $\mathrm{tr}\rho^2$. The concurrence goes to zero asymptotically.

For initial state II, however, the entanglement behaves very differently: The concurrence goes to zero for $p < 1$, thus demonstrating "entanglement sudden death." We stress that the onset of separability ($C = 0$) occurs at the same point for all entanglement quantifiers and is not a particular artifact of the concurrence.

It is also illustrative to study the purity, defined as $\mathrm{tr}\rho^2$, as a function of the decay probability (Fig. 3) for states I and II. In both cases the purity reaches a minimum but is restored when $p = 1$, when all photons have "decayed" to the H-polarization state. State II is more mixed than state I in the intermediate stages of this process because it has a larger $|VV\rangle$ component and thus becomes more entangled with the environment.

To further illustrate the usefulness of the present scheme for studying decoherence of entangled systems, we performed a second experiment studying the phase-damping channel, described by the map (*1*):

$$|g\rangle_S \otimes |0\rangle_R \rightarrow |g\rangle_S \otimes |0\rangle_R$$
$$|e\rangle_S \otimes |0\rangle_R \rightarrow \sqrt{1-p}\,|e\rangle_S \otimes |0\rangle_R + \sqrt{p}\,|e\rangle_S \otimes |1\rangle_R \quad (6)$$

This map could represent elastic scattering between atom and reservoir. States $|e\rangle$ and $|g\rangle$ are not changed by the interaction, but any coherent superposition of them gets entangled with the reservoir. There is no longer decay, but only loss of coherence between ground and excited states. The dephasing map can be implemented with the same interferometer through the addition of an extra HWP at 45° in mode b before the QST system (or, equivalently, through the removal of HWP3 and redefinition of the QST measurements). For the dephasing channel, pure states I and II present identical behavior, becoming completely disentangled only when $p = 1$. Figure 4 shows the concurrence (squares) and bipartite purity (triangles) as a function of p for the entangled state II.

In demonstrating the sudden disappearance of the entanglement of a bipartite system, induced by the interaction with an environment, our results show that entangled states with the same initial concurrence may exhibit, for the same reservoir, either an abrupt or an asymptotic disappearance of entanglement, even though the constituents of the system always exhibit an asymptotic decay. We have explicitly shown that this behavior also depends on the characteristics of the reservoir through two examples corresponding to amplitude decay and dephasing. The experimental setup represents a reliable and simple method for studying the dynamics of entangled systems interacting with controlled environments.

References and Notes

1. M. Nielsen, I. Chuang, *Quantum Computation and Quantum Information* (Cambridge Univ. Press, Cambridge, 2000).
2. C. H. Bennett, D. P. DiVincenzo, *Nature* **404**, 247 (2000).
3. C. H. Bennett, G. Brassard, *Proceedings of the International Conference on Computer Systems and Signal Processing, Bangalore, India* (IEEE, New York, 1984), pp. 175–179.
4. A. K. Ekert, *Phys. Rev. Lett.* **67**, 661 (1991).
5. N. Gisin, G. Ribordy, W. Tittel, H. Zbinden, *Rev. Mod. Phys.* **74**, 145 (2002).
6. C. H. Bennett *et al.*, *Phys. Rev. Lett.* **70**, 1895 (1993).
7. D. Bouwmeester *et al.*, *Nature* **390**, 575 (1997).
8. D. Boschi, S. Branca, F. DeMartini, L. Hardy, S. Popescu, *Phys. Rev. Lett.* **80**, 1121 (1998).
9. L.-M. Duan, M. D. Lukin, J. I. Cirac, P. Zoller, *Nature* **414**, 413 (2001).
10. W. H. Zurek, *Rev. Mod. Phys.* **75**, 715 (2003).
11. L. Diósi, in *Irreversible Quantum Dynamics*, F. Benatti, R. Floreanini, Eds. (Springer, Berlin, 2003), pp. 157–164.
12. P. J. Dodd, J. J. Halliwell, *Phys. Rev. A* **69**, 052105 (2004).
13. T. Yu, J. H. Eberly, *Phys. Rev. Lett.* **93**, 140404 (2004).
14. M. F. Santos, P. Milman, L. Davidovich, N. Zagury, *Phys. Rev. A* **73**, 040305 (2006).
15. T. Yu, J. H. Eberly, *Phys. Rev. Lett.* **97**, 140403 (2006).
16. W. K. Wootters, *Phys. Rev. Lett.* **80**, 2245 (1998).
17. A similar configuration, but with the addition of cylindrical lenses, was used to realize a direct measurement of entanglement for a pure state in (*21*).
18. D. F. V. James, P. G. Kwiat, W. J. Munro, A. G. White, *Phys. Rev. A* **64**, 052312 (2001).
19. P. G. Kwiat, E. Waks, A. G. White, I. Appelbaum, P. H. Eberhard, *Phys. Rev. A* **60**, R773 (1999).
20. J. B. Altepeter, E. R. Jeffrey, P. G. Kwiat, in *Advances in Atomic, Molecular and Optical Physics*, P. Berman, C. Lin, Eds. (Elsevier, San Diego, CA, 2005), vol. 52, pp. 107–161.
21. S. P. Walborn, P. H. S. Ribeiro, L. Davidovich, F. Mintert, A. Buchleitner, *Nature* **440**, 1022 (2006).

22. Supported by the Brazilian funding agencies CNPq, CAPES, PRONEX, FUJB, and FAPER]. This work was performed as part of the Brazilian Millennium Institute for Quantum Information.

12 January 2007; accepted 20 March 2007
10.1126/science.1139892

Enantioselective Organocatalysis Using SOMO Activation

Teresa D. Beeson,[1,2] Anthony Mastracchio,[1,2] Jun-Bae Hong,[1,2] Kate Ashton,[1,2] David W. C. MacMillan[1,2]*

The asymmetric α-addition of relatively nonpolar hydrocarbon substrates, such as allyl and aryl groups, to aldehydes and ketones remains a largely unsolved problem in organic synthesis, despite the wide potential utility of direct routes to such products. We reasoned that well-established chiral amine catalysis, which activates aldehydes toward electrophile addition by enamine formation, could be expanded to this important reaction class by applying a single-electron oxidant to create a transient radical species from the enamine. We demonstrated the concept of singly occupied molecular orbital (SOMO) activation with a highly selective α-allylation of aldehydes, and we here present preliminary results for enantioselective heteroarylations and cyclization/halogenation cascades.

Over the past four decades, the capacity to induce asymmetric transformations with enantioselective catalysts has remained a focal point for extensive research efforts in both industrial and academic settings. During this time, thousands of asymmetric catalytic reactions have been invented (*1*), in accord with the increasing need for enantiopure medicinal agents and the rapid advancement of the field of asymmetric synthesis. Most catalytic enantioinductive processes are derived from a small number of long-established activation modes. Activation modes such as Lewis acid catalysis (*2*), σ-bond insertion (*3*), π-bond insertion (*4*), atom transfer catalysis (*5*), and hydrogen bonding catalysis (*6*) have each spawned countless asymmetric reaction classes, thereby dramatically expanding the synthetic toolbox available to researchers in the physical and biological sciences. A necessary objective, therefore, for the continued advancement of the field of chemical synthesis is the design and implementation of distinct catalytic-activation modes that enable previously unknown transformations.

Over the past 8 years, our laboratory has been involved in the development of the field of organocatalysis, a research area that relies on the use of small organic molecules as catalysts for enantioselective transformations. As part of these studies, we introduced the concept of iminium catalysis (*7*): an enal or enone activation mode that lowers the energy of the substrate's lowest unoccupied molecular orbital, facilitating enantioselective C–C and C–N conjugate additions, cycloadditions, hydrogenations, and Friedel-Crafts alkylations (*8*). Simultaneously, Barbas and List (*9*) brought to fruition the concept of enamine catalysis (Fig. 1), which raises the energy of the highest occupied molecular orbital (HOMO) in aldehydes and ketones to promote enantioselective α-carbonyl functionalization with a large range of electrophiles (*10*). These two modes of catalyst activation (iminium and enamine) have provided, in total, more than 60 asymmetric methodologies over the past 7 years.

[1]Merck Center for Catalysis, Department of Chemistry, Princeton University, Princeton, NJ 08544, USA. [2]Division of Chemistry and Chemical Engineering, California Institute of Technology, Pasadena, CA 91125, USA.

*To whom correspondence should be addressed. E-mail: dmacmill@princeton.edu